

Electron capture in $\text{Ar}^+ + \text{H}_2$ collisions in the keV energy regimeM. Kimura,* S. Chapman,[†] and N. F. Lane[‡]*Joint Institute for Laboratory Astrophysics, University of Colorado and National Bureau of Standards, Boulder, Colorado 80309*

(Received 20 May 1985)

Electron capture in $\text{Ar}^+(^2P) + \text{H}_2(X^1\Sigma_g)$ collisions in the keV energy regime has been studied theoretically. The molecular-orbital expansion method was used within a semiclassical formalism and an electron translation factor correction was incorporated to the first order in the magnitude of the relative velocity \mathbf{V} . The molecular wave function and eigenenergy were obtained using the diatoms-in-molecules (DIM) method. We have examined the effect of the orientation of the target H_2 molecule on the electron-capture mechanism within the sudden adiabatic approximation. Since π symmetry arising from the p orbital of the Ar^+ ion is involved in this system, a strong influence on the probability of the molecular orientation was found in all energies studied. As the collision energy increases, the Π -symmetry state in the initial channel becomes more important through the rotational coupling to the electron-capture mechanism, while at lower energies the Σ -symmetry state in the initial channel is the dominant source for the electron capture through strong radial coupling. Agreement of the present theory with measurements is good, but marked disagreement is seen with the atomic-orbital calculation.

I. INTRODUCTION

The dynamics of various events in $\text{Ar}^+ + \text{H}_2$ collisions in the eV energy region has been the subject of extensive experimental as well as theoretical investigations,^{1,2} particularly in theoretical chemistry. Within the Born-Oppenheimer approximation, potential-energy surfaces of the ArH_2^+ system were computed using the diatoms-in-molecules (DIM) method.^{3,4} This DIM method, though not a pure *ab initio* method, has been demonstrated to offer "reasonably accurate" wave functions and eigenvalues for such a simple technique. Chapman and Preston¹ have applied the trajectory-surface-hopping method with the DIM potential surfaces to investigate electron capture and rearrangement (chemical reaction) processes in $\text{Ar}^+ + \text{H}_2$ collisions with much success. In the energy range $E \geq 100$ eV, one previous theoretical attempt to study the electron-capture mechanism in $\text{Ar}^+ + \text{H}_2$ collisions using the atomic-orbital (AO) expansion method has been reported by Hedrick *et al.*⁵ These authors employed the two-center AO expansion method *without* the use of an electron-translation factor (ETF). As they were interested in low energies, neglect of the ETF might be justifiable practically (though questionable theoretically). However, it is our view that a molecular treatment is more appropriate at such low energies. Furthermore, for some cases it is known that a simple two-center AO expansion method introduces serious error in interpreting the collision dynamics,⁶ since this method does not account for the relaxation of the electron orbitals during close collisions. Aside from the work of Ref. 5, no rigorous theoretical study of the collision dynamics in $\text{Ar}^+ + \text{H}_2$ collisions has been made, in contrast to experimental prosperity in this field.

We have performed a theoretical study of electron capture in $\text{Ar}^+ + \text{H}_2$ collisions using a three-state molecular-

orbital (MO) expansion method incorporating ETF corrections within a semiclassical formalism. The molecular wave functions and adiabatic potential curves were obtained by the DIM method. We have also examined the effect of orientation of the target H_2 molecule on the electron-capture probabilities.

II. THEORETICAL METHOD

Since the details of the theoretical treatment used here have been described elsewhere,⁷ only a summary will be given here. Molecular wave functions and corresponding eigenenergies have been obtained by using the DIM method.^{3,4} Based on the valence-bond ideas, the DIM method has been widely used recently because of its simplicity and ability in generating "reasonably accurate" potential surfaces for polyatomic systems.^{7,8} In the DIM method, the electron Hamiltonian is partitioned into atomic and diatomic terms. This partitioning of the electronic Hamiltonian is *exact*. Probably the most crucial approximation used in the DIM method is the fact that the partitioned atomic and diatomic fragments are fully determined by using properties of the isolated fragments. Also, zero overlap (ZO) of the atomic orbitals is usually assumed. The approximation in the method are most reliable at large separations, but, depending on the size of the basis, they may fail seriously when the fragments interact strongly, e.g., at small separations. Nevertheless, quite good agreement with large scale *ab initio* calculations has been obtained for molecular geometries and energies.⁴ In our view, however, the critical collision dynamics usually take place at relatively "large" internuclear separation, i.e., $R \geq R_e$, where the DIM surfaces are most reliable. Another important factor in the theoretical description of the collision dynamics is the accurate inclusion of the asymptotic adiabatic energy defect between the initial and final states (this is automatically guaranteed in the DIM

method), and these facts might compensate for defects that the DIM method might have. In the present case, careful studies¹⁻³ of the accuracy of potential surfaces of the ArH_2^+ system obtained by using the DIM method support their validity.

The scattering wave function is then expanded in terms of products of the Born-Oppenheimer wave functions (DIM wave functions), the vibrational wave functions of the target molecule, and the electron-translation factors (ETF). The ETF describes the translation effect of the electron moving with a particular nucleus or molecule, and ensures that the scattering wave functions satisfy the correct scattering boundary conditions. The inclusion of the ETF in the expansion is not only a matter of formality, but also of practical importance.^{9,10} Without the ETF, the coupling matrix shows origin dependence of the chosen electron coordinate; hence the calculated probability cannot be determined uniquely, at least with a small basis.

Substituting the scattering wave function into the time-dependent Schrödinger equation, expanding the ETF in terms of the relative velocity \mathbf{V} , and retaining the first-order term of \mathbf{V} (this approximation may be quite valid in the present energy range, see Ref. 10), one obtains the first-order coupled equations similar to those seen in ion-atom scattering problems,¹⁰ except for the presence of overlap terms involving the vibrational wave functions of the target molecule. These coupled equations have to be solved numerically. In the rotating coordinate frame, the coupling matrix consists of radial coupling and rotational coupling parts. One approximation made in deriving the coupled equations is the assumption of classical trajectories; this is consistent with the present study of the dynamics in $\text{Ar}^+ + \text{H}_2$ collisions in the keV energy region. Since the collision energies of interest here are exceedingly large compared to the vibrational and rotational energies of the molecule, the sudden adiabatic approximation applied to the nuclear motion of the molecule also is valid. Thus, the diatomic nuclear motion is frozen at its equilibrium distance $R_e = 1.401a_0$ during the collision, and the Franck-Condon approximation is employed to describe nuclear transitions between the $\text{H}_2(X^1\Sigma_g)$ and $\text{H}_2^+(1S\sigma_g)$ states. The vibrational overlap matrix elements that occur in the coupled equations were evaluated numerically for the final vibrational states $v'=0-20$. Therefore, most of the results shown below have been performed by summing up the final vibrational states to $v'=20$.

To check the validity of the sudden adiabatic approximation, several calculations were carried out at different internuclear separations $R_{\text{H-H}}$ of the target H_2 molecule and consequently, different energy gaps and couplings. The cross sections obtained by averaging the cross sections calculated at a few $R_{\text{H-H}}$ values differ by only 12% from those obtained by fixing $R_{\text{H-H}}$ at R_e .

III. RESULTS AND DISCUSSIONS

The coordinates of the colliding system are shown in Fig. 1. The angles θ and ϕ are defined as the polar and azimuthal angles, respectively, in a spherical coordinate system.

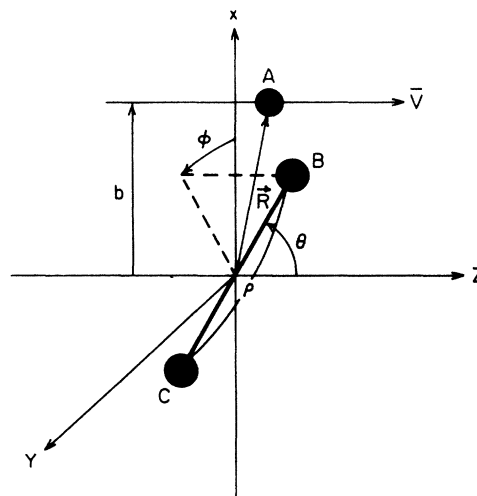


FIG. 1. Coordinate in the laboratory frame for the $\text{Ar}^+ + \text{H}_2$ system.

All calculations have been carried out by means of a three-state MO close-coupling method (initial $[\text{Ar}^+(^2P) + \text{H}_2(X^1\Sigma_g)]$ and final $[\text{Ar}(^1S) + \text{H}_2^+(1S\sigma_g)]$ states) with a screened Coulomb trajectory for the heavy particle path. Also, we have neglected the spin-orbit splitting which gives rise to $^2P_{3/2}$ and $^2P_{1/2}$ states of the Ar^+ ion. The results described below are "averaged" arising from these two J states.

A. Adiabatic potentials

Figure 2 depicts adiabatic potential curves on the ArH_2^+ system with different orientations θ and fixed $\phi=0$. The two states correlating with the $[\text{Ar}^+(^2P) + \text{H}_2(X^1\Sigma_g)]$ state result from σ and π symmetries of the p orbital in the Ar^+ ion, while only one (σ type) symmetry is present in the charge-transfer channel $[\text{Ar}(^1S) + \text{H}_2^+(1S\sigma_g)]$.

The two states in the initial channel are, of course, degenerate at infinite R separation. It should be noted that the 1Σ state has an unexpected slight hump with the magnitude approximately 0.004 a.u. around $R=7a_0$. Although we are not sure of the cause of this hump, it is most likely due to the strong mixing ("avoided crossing") of two different states, 1Σ and 2Σ , which have the same (Σ) symmetry with a small-energy separation [the difference of energy between 1Σ and 2Σ states at $R\sim 7a_0$ is only ~ 0.027 a.u. (or ~ 0.75 eV)]. Alternatively, the barrier may be an artifact of the DIM method due to the breakdown of this method at small R .

The influence of the orientation of the H_2 molecule is also noticeable, in particular, for the 1Σ state. As the angle θ increases, the position of the minimum as well as that of the hump shifts toward smaller R (the maximum difference is about 6%).

The orientation effect seen in the 1Π state can be attributed to the fact that because of the Π character of the p orbital of the Ar^+ ion, the charge clouds of the Ar^+ ion

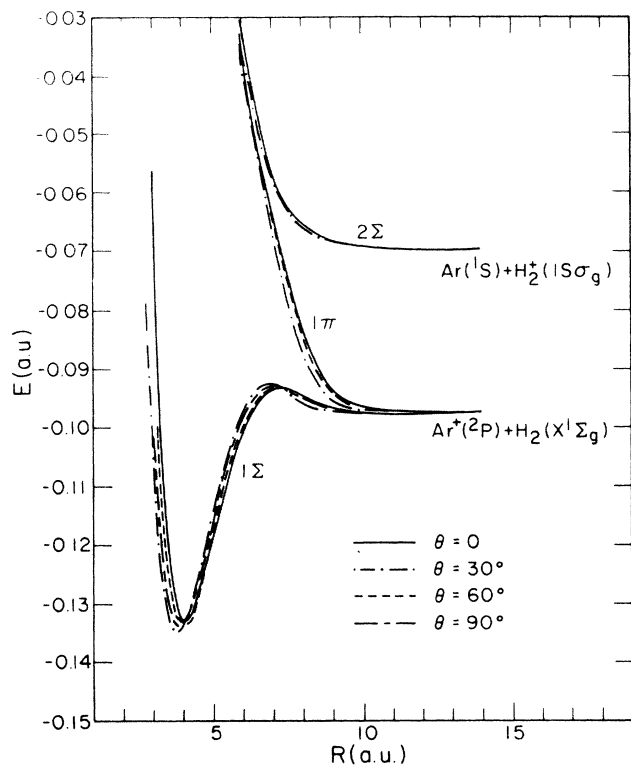


FIG. 2. Adiabatic potentials as function of internuclear coordinate R and angle θ , between the molecular axis and internuclear coordinate. The azimuthal angle ϕ is fixed with 0° .

and the H_2 molecule do not experience strong overlap except for small separations. The same argument, but this time the other way around, applies to a less pronounced feature of the orientation effect observed in the 2Σ state, since the 2Σ state has spherically symmetric charge clouds around both nuclei.

It may be worthwhile noting that the energy curves of the 1Π and 2Σ states do not cross for any orientation within the R range we calculated. Adiabatic potential curves for different orientations ϕ but with fixed θ (not shown) are similar to those shown in Fig. 2, but the influence of the ϕ orientation on the curves is less pronounced.

B. Coupling and electron-capture mechanism

Radial-coupling matrix element that connect the 1Σ and 2Σ states are plotted for different values of θ and fixed $\phi=0^\circ$ in Fig. 3, and for different ϕ values but with fixed $\theta=60^\circ$ in Fig. 4. Rotational couplings between 1Π and 2Σ states with different θ values and fixed $\phi=0^\circ$ are plotted in Fig. 5.

First, consider Fig. 3. The radial coupling has two sharp peaks at $R \sim 2.5$ and $R \sim 6.5a_0$ to $7.5a_0$ with the smaller peak at the smaller R and the larger peak at the larger R . The larger peak at $R \sim (6.5-7.5)a_0$ is apparently due to Demkov coupling which is characteristic of near-resonant electronic states and is expected to play a dominant role in the electron-capture mechanism. The smaller peak at $R \sim 2.5a_0$ results from the mixture of the electronic states at small R and may be secondary. As the curves clearly show, the effect of the orientation of the target molecule on the radial coupling is remarkable. The largest difference in magnitude, viz., between the coupling at $\theta=0^\circ$ and that of $\theta=60^\circ$ is approximately a factor of 2. Also, the position of the maximum lies at $R \sim 6.6a_0$ and $7.5a_0$ for $\theta=0^\circ$ and 60° , respectively, and correspondingly, the coupling at $\theta=60^\circ$ is larger in size.

Turning to Fig. 4, radial couplings with different ϕ values have two peaks, viz., at $R \sim 2.5a_0$ and $7.5a_0$ as previously. However, in contrast to Fig. 3, all the couplings in Fig. 4 look almost identical except for slight differences in the smaller peak at $R \sim 2.5a_0$. This similarity of couplings both in magnitude and shape due to

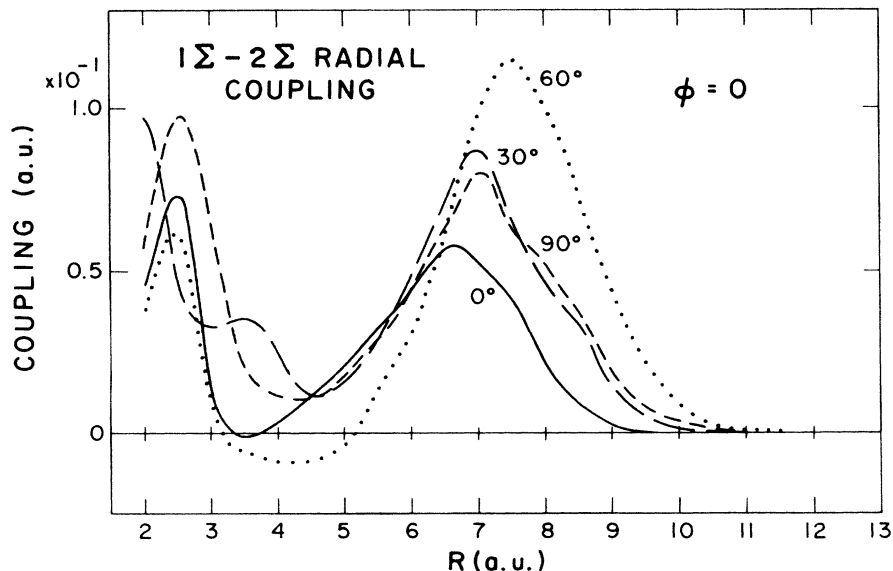


FIG. 3. Radial couplings between 1Σ and 2Σ states with varying θ (fixed $\phi=0^\circ$).

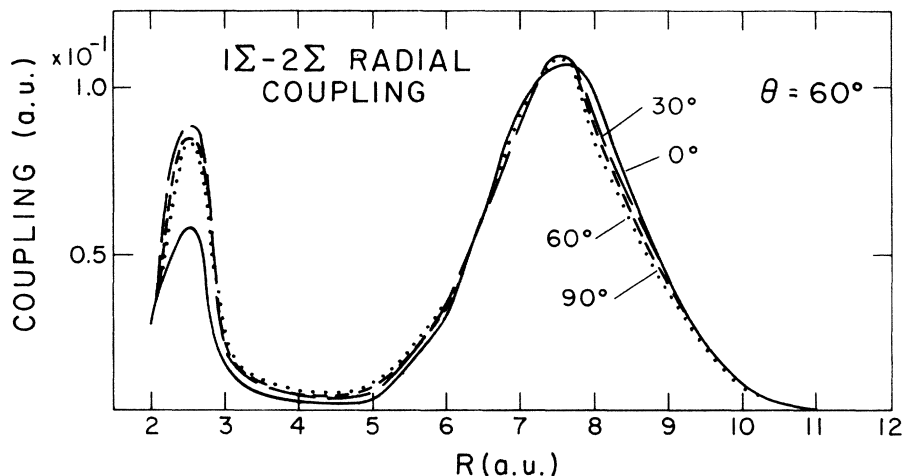


FIG. 4. Radial couplings between 1Σ and 2Σ states with varying ϕ (fixed $\theta = 60^\circ$).

“accidental degeneracy”⁷ suggests that the ϕ dependence in the calculated probabilities and hence, in the cross sections, may be expected to be very weak. Indeed, as is discussed later, the influence of ϕ orientation on the probability is found to be small.

Rotational couplings shown in Fig. 5 also show strong effects of the θ orientation, although they join each other for $R \geq 3a_0$. The coupling at $\theta = 60^\circ$ is about a factor of 2 smaller in magnitude than others in this R region. In general, the rotational coupling is important only at small R , unless the two states considered experience an actual curve crossing at an intermediate internuclear separation.

To examine details of the electron-capture dynamics, two separate two-state close-coupling calculations, namely 1Σ - 2Σ and 1Π - 2Σ , were performed at the collision energy $E = 1$ keV, and impact parameter $b = 2a_0$. The time evo-

lution of the charge-transfer probability for various orientations θ is displayed in Fig. 6 and 7 for 1Σ - 2Σ and 1Π - 2Σ , respectively. In the 1Σ - 2Σ calculation the probabilities start rising at $t \approx -200$ a.u. (or $R \approx 6.6a_0$) regardless of the orientation θ . This corresponds exactly to the location of the largest peak in the radial coupling. Although small oscillations of the probabilities can be observed in the period $-180 \leq t \leq +180$ a.u., the colliding particles experience virtually no interaction; i.e., “nothing serious” happens during this period. When the projectile enters the strong-interaction region along the exit path, again the probabilities oscillate strongly until the electron selects the final state. This picture reveals explicitly that in this energy regime, radial coupling is important in the region where the matrix element possesses the largest maximum. On the other hand, the probabilities in the 1Π - 2Σ calcula-

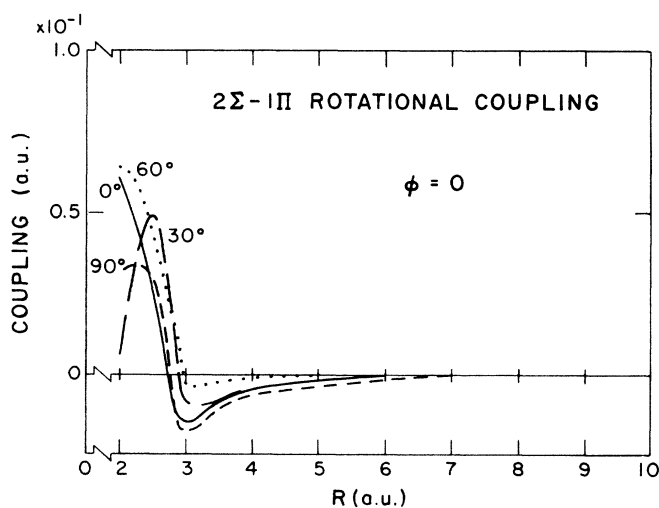


FIG. 5. Angular couplings between 1Π and 2Σ states with varying θ (fixed $\phi = 0^\circ$).

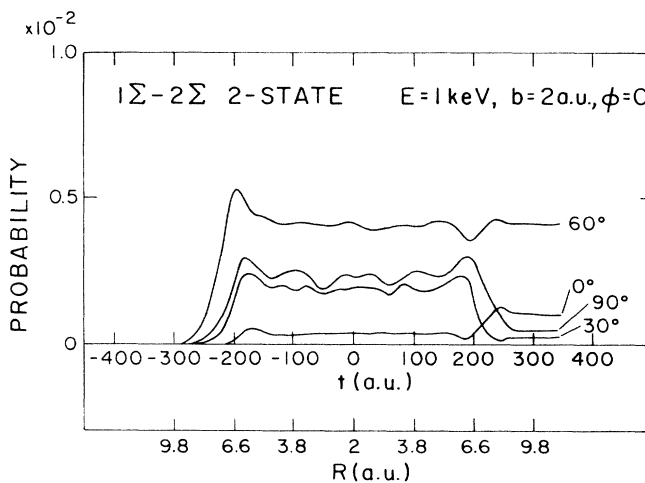


FIG. 6. Time-evolution study in 1Σ - 2Σ two-state calculation at $E = 1$ keV, $b = 2.0$, and $\phi = 0^\circ$.

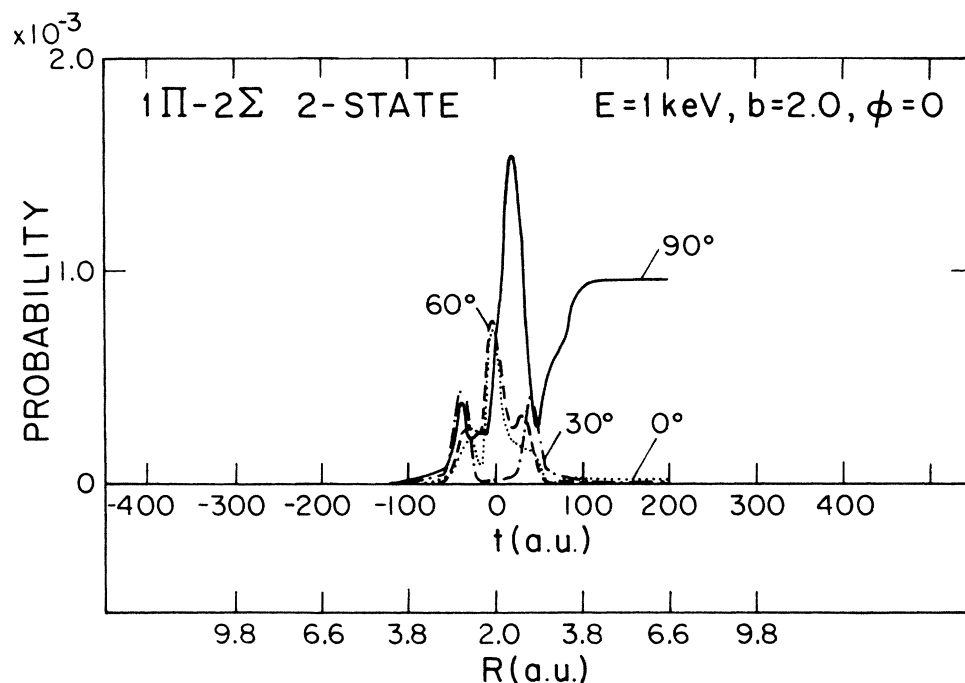


FIG. 7. Time-evolution study in $1\Pi-2\Sigma$ two-state calculation at $E=1$ keV, $b=2.0$, and $\phi=0^\circ$.

tion oscillate during the period $-100 \leq t \leq +100$ a.u. (or $R \leq 3.8a_0$) where the colliding particles interact strongly through rotational coupling, since the corresponding matrix elements, shown in Fig. 7, are large only in this region. Comparing Figs. 6 and 7, it is evident that the two interaction regions, where the radial coupling and rotational coupling are effective, are quite well separated. In

both cases the magnitude of the probability is directly related to that of the appropriate coupling matrix element. The time evolutions of the probabilities corresponding to a three-state MO close-coupling calculation are displayed in Fig. 8. Even with this expanded basis set, the regions where the radial and rotational coupling contribute to the electron-capture process still are well isolated in spite of

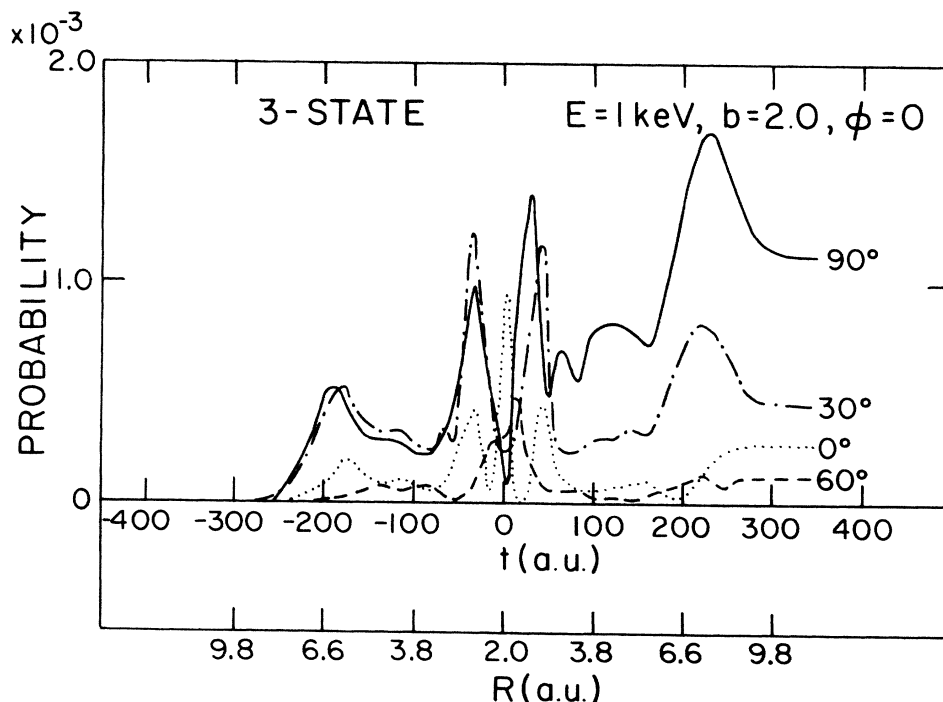


FIG. 8. Time-evolution study in three-state calculation of $E=1$ keV, $b=2.0$, and $\phi=0^\circ$.

TABLE I. Two-state cross section for $\text{Ar}^+(^2P) + \text{H}_2(X^1\Sigma_g, v=0) \rightarrow \text{Ar}(^1S) + \text{H}_2^+(1S\sigma_g; v'=2)^a$; $\phi=0^\circ$. Σ - Σ represents the 1Σ - 2Σ two state result and similarly Π - Σ is the 1Π - 2Σ state result.

E (keV)	Cross section (10^{-16} cm 2)							
	$\theta=0^\circ$		$\theta=30^\circ$		$\theta=60^\circ$		$\theta=90^\circ$	
	Σ - Σ	Π - Σ	Σ - Σ	Π - Σ	Σ - Σ	Π - Σ	Σ - Σ	Π - Σ
0.4	2.04^{-2}	1.48^{-3}	2.87^{-2}	3.62^{-4}	4.21^{-2}	1.36^{-3}	1.16^{-2}	5.43^{-4}
1.0	1.64^{-2}	2.53^{-3}	2.97^{-2}	5.24^{-4}	4.20^{-2}	2.31^{-3}	1.10^{-2}	9.82^{-4}
4.0	1.59^{-2}	9.76^{-3}	3.49^{-2}	1.59^{-3}	4.18^{-2}	8.36^{-3}	1.01^{-2}	3.53^{-3}

^aThe vibrational transition $v=0 \rightarrow v'=2$ is chosen as an example because it has the largest vibrational overlap matrix element.

the additional rotational coupling between the two initial states. Enhancement effects on the probabilities due to the additional 1Π state are clearly seen at $|t| \leq 100$ a.u. The 1Σ - 1Π rotational coupling is of importance as the 1Π state serves as a "flux container."

C. Cross section

Some representative cross sections obtained by the two-state close-coupling calculations are given in Table I. The orientation effects on the calculated cross sections in both two-state calculations are quite apparent. The difference between the largest cross section, which occurs at $\theta=60^\circ$, and the smallest, at $\theta=90^\circ$, is about a factor of 4 at $E=4$ keV. This difference is reduced to a factor of 3 at $E=0.4$ keV.

Also apparent is the importance of the Π -symmetry contribution to the electron-capture cross section. In general, regardless of the molecular orientation, the cross section obtained by the Π - Σ two-state calculation increases rapidly as the collision energy increases, while that of the Σ - Σ two-state calculation shows relative insensitivity to the collision energy. For example, at $\theta=60^\circ$, the $\sigma_{\Pi-\Sigma}/\sigma_{\Sigma-\Sigma}$ ratio increases from 3.23×10^{-2} to 2.0×10^{-1} as the energy is increased from 0.4 to 4.0 keV. This ratio exceeds unity when the collision energy is at 40 keV (not reported). The 1Π state is asymptotically degenerate with the 1Σ state, and these two states are connected through strong rotational coupling (see Fig. 2). Therefore, although the 1Π state as a single initial channel does not seem to play an important direct role in electron capture at lower energies, it is important as a "flux server" when the 1Π state is combined with the 1Σ state, both in the initial channel. This was demonstrated in Fig. 8 as the enhancement effect of the probability in the time-evolution study.

TABLE II. Three-state cross section for $\text{Ar}^+(^2P) + \text{H}_2(X^1\Sigma_g; v=0) \rightarrow \text{Ar}(^1S) + \text{H}_2^+(1S\sigma_g; v'=2)$; $\phi=0^\circ$.

E (keV)	Cross section (10^{-16} cm 2)			
	$\theta=0^\circ$	$\theta=30^\circ$	$\theta=60^\circ$	$\theta=90^\circ$
0.4	2.09^{-2}	2.05^{-2}	4.33^{-2}	1.04^{-2}
1.0	2.11^{-2}	2.01^{-2}	4.12^{-2}	1.10^{-2}
4.0	2.11^{-2}	1.89^{-2}	3.95^{-2}	8.55^{-3}

The cross sections obtained by three-state close-coupling calculations are listed in Table II. Again, the effect of the orientation of the target H_2 molecule is found to be very strong. The ratio of the largest cross section at $\theta=60^\circ$ to the smallest at $\theta=90^\circ$ is nearly 4.6 at $E=4$ keV. Although this ratio varies with the collision energy, values ranging from 2 to 3 prevail at all the energies studied. This behavior is most likely the result of the presence of the open p orbital in the Ar^+ ion in the initial channel, and is quite different from that found in the $\text{H}^+ + \text{H}_2$ collision study,⁷ in which both initial and final states involve only spherically symmetry electron densities. Also, the cross section is fairly constant as a function of the collision energy in the $\text{Ar}^+ + \text{H}_2$ collision, in contrast to the $\text{H}^+ - \text{H}_2$ system.⁷

We have calculated the total electron-capture cross section as a function of the collision energy (after integrating over angles θ and ϕ). Calculated results are shown in Fig. 9 along with some experimental measurements^{5,11-13} and other theoretical results.⁵

Our results lie about 20% higher than the measurements of Amme and McIlwain¹¹ in the energy range 0.6–1 keV, although the qualitative shape of the cross-section curve is in reasonably good accord.

The present result lies as much as 15% below the measurement by Hedrick *et al.*,⁵ below 1.5 keV, and consistently (within 10%) higher than the same measurement in the energy region $1.5 \leq E < 3$ keV. The present result

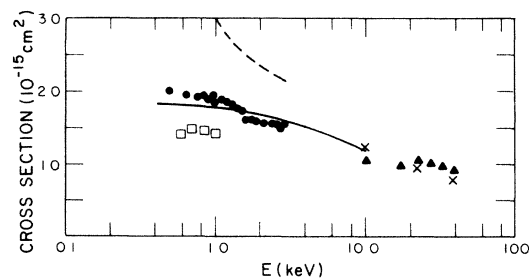


FIG. 9. Electron-capture cross section for $\text{Ar}^+ + \text{H}_2(X^1\Sigma_g, v=0) \rightarrow \text{Ar} + \text{H}_2^+(1S\sigma_g, v'=1-20)$. Theory: solid line, present; dashed line, AO result, Ref. 5. Experiment: \square , Ref. 11; \bullet , Ref. 5; \blacktriangle , Ref. 12; \times , Ref. 13.

ties nicely to the single data point at 10 keV, which is the lowest energy point of Latimer's measurements,¹² and also ties to that of Gilbody and Hasted.¹³

Comparing the theoretical result by Hedrick *et al.*,⁵ who used the AO expansion method *without* the ETF, one finds considerable disagreement between the two theories. Their cross section differs by about a factor of 1.7 at 1 keV, and although this factor is reduced to 1.3 at 3 keV, the qualitative shape of the cross section is entirely different. In the low-energy region where the ETF is expected to be less important in the AO expansion method, the MO expansion method is certainly superior to the AO method, since the AO method cannot allow for electron relaxation. As the energy increases, the neglect of the ETF from the AO expansion is defective and the results cannot be accurate. In fact, there might be no energy re-

gion in which the AO expansion method without ETF is valid unless a "near" complete set is employed. From this point of view, the present results should be more reliable. Overall agreement of the present results with all measurements are satisfactory. However, the neglect of other inelastic channels, such as vibrational excitation, which is expected to be a dominant channel in a low-energy collision, introduces some uncertainty in assessing the accuracy of our theoretical results.

ACKNOWLEDGMENT

Two of us (M.K. and N.F.L.) were supported by the U.S. Department of Energy, Office of Basic Energy Sciences.

*Also at Department of Physics, Rice University, Houston, TX 77001.

†Permanent address: Department of Chemistry, Barnard College, Columbia University, New York, NY 10027.

‡Also at University of Colorado, Colorado Springs, and at Rice University, Houston, TX 77001.

¹S. Chapman and R. K. Preston, *J. Chem. Phys.* **60**, 650 (1974).

²S. Chapman, *J. Chem. Phys.* **82**, 4033 (1985).

³P. J. Kuntz and A. C. Roach, *J. Chem. Soc. Faraday Trans. 2* **68**, 259 (1972).

⁴J. C. Tully, *J. Chem. Phys.* **58**, 1396 (1973).

⁵A. F. Hedrick, T. F. Moran, K. J. McCann, and M. R. Flannery, *J. Chem. Phys.* **66**, 24 (1977).

⁶See, for example, W. Fritsch and C. D. Lin, *Phys. Rev. A* **26**, 762 (1982).

⁷M. Kimura, *Phys. Rev. A* **32**, 802 (1985).

⁸R. D. Piacentini and A. Salin, *J. Phys. B* **11**, L323 (1978).

⁹J. B. Delos and W. R. Thorson, *J. Chem. Phys.* **70**, 1774 (1979).

¹⁰See, for example, M. Kimura and W. R. Thorsen, *Phys. Rev. A* **24**, 1780 (1981).

¹¹R. C. Amme and J. F. McIlwain, *J. Chem. Phys.* **45**, 1224 (1966).

¹²C. J. Latimer, *J. Phys. B* **10**, 515 (1977).

¹³H. B. Gilbody and J. B. Hasted, *Proc. R. Soc. London Ser. A* **238**, 334 (1956).